Research Article | Vol. 26, No. 17 | 20 Aug 2018 | OPTICS EXPRESS 21700
Optics EXPRESS

Miniature fiber-optic high-intensity focused ultrasound device using a candle soot nanoparticles-polydimethylsiloxane composites-coated photoacoustic lens

YAO LI,[1] ZHENDONG GUO,[1] GUANGYAO LI,[1] AND SUNG-LIANG CHEN[1,2,*]

[1]*University of Michigan-Shanghai Jiao Tong University Joint Institute, Shanghai Jiao Tong University, Shanghai 200240, China*
[2]*State Key Laboratory of Advanced Optical Communication Systems and Networks, Shanghai Jiao Tong University, Shanghai 200240, China*
[*]*sungliang.chen@sjtu.edu.cn*

Abstract: We present a miniature fiber-optic ultrasound transmitter for generating high-intensity focused ultrasound (HIFU) based on photoacoustic transduction. The HIFU device consists of a fiber and a photoacoustic lens. We develop a simple fabrication procedure for making the photoacoustic lens, which is coated with candle soot nanoparticles-polydimethylsiloxane composites. The fiber is used to deliver pulsed laser for photoacoustic excitation, which facilitates the use of the HIFU device by eliminating the need of free-space optical alignment. The HIFU device (6.5 mm in diameter) produces focused acoustic pressures up to >30 MPa in peak positive with a tight −6-dB focal volume of ~100 μm and ~500 μm in the lateral and axial directions, respectively. Acoustic cavitation induced by the HIFU device is demonstrated. The miniature HIFU device facilitates handheld operation. It holds promise for clinical applications in intraoperative high-precision HIFU therapy. It can even be used for intracavitary therapy with further miniaturization.

1. Introduction

High-intensity focused ultrasound (HIFU) is a medical technology that is currently developed worldwide to treat a range of disorders. By concentrating ultrasound within a focal volume through an acoustic lens, HIFU can provide useful thermal or mechanical effects on a target. HIFU has been used in a wide range of applications such as treatment of liver and kidney tumors [1], targeting and delivery of drugs [2], and ablation of bones [3]. Moreover, cavitation-based HIFU can enhance therapeutic efficacy and has shown promising applications such as tumor growth reduction [4]. Image-guided HIFU therapy is typically performed to enable targeting and monitoring during treatment.

Piezoelectric transducers are commonly used for HIFU generation. Their center frequencies are typically several MHz, and their apertures are several centimeters, which results in a focal spot size of >1 mm in diameter. Localized heating generated by the piezoelectric transducer can be used to treat cysts and tumors, benign or malignant. However, there are limitations in clinical applications by the piezoelectric transducer. (i) High-precision targeted therapy is highly challenging due to the large focal spot size of the piezoelectric transducer. Tumors are often grown in the vicinity of vital blood vessels that should not be impaired by HIFU [5]. Thus, a tiny focal spot size of HIFU for selective treatment is desired. The tiny focal spot size can be realized by high-frequency (tens of MHz) focused ultrasound, yet the fabrication of the high-frequency focused piezoelectric transducer is technically challenging, especially for HIFU generation. (ii) Intraoperative operation is hampered due to the large aperture size of the piezoelectric transducer.

Other than conventional piezoelectric transducers for ultrasound generation, laser-generated ultrasound (LGUS) transmitters are attractive candidates for advanced ultrasound

#334876 https://doi.org/10.1364/OE.26.021700
Journal © 2018 Received 11 Jun 2018; revised 13 Jul 2018; accepted 20 Jul 2018; published 7 Aug 2018

Optics EXPRESS

applications [5–29]. Besides the visible laser wavelengths, LGUS excited at the terahertz regime have also been explored [13]. LGUS is based on photoacoustic effect. The transmitter absorbs the optical energy from a pulsed laser, which is then converted into localized and transient temperature rise. The temperature rise causes thermal expansion of the transmitter and finally, pulsed acoustic waves are generated. Although the energy conversion efficiency of LGUS transmitters is poor (~4×10^{-3} [18]), the LGUS method could easily generate high-frequency broadband ultrasound from tens of MHz to even GHz. Thus, development of LGUS transmitters has drawn increasing attention in the past few years. A variety of flat LGUS transmitters were investigated using metallic or carbon-based absorbers [6–9,17–19,21]. The efficiency has been improved in the past few years. For example, candle soot nanoparticles (CSNPs)-polydimethylsiloxane (PDMS) composites achieved relatively high energy conversion efficiency [18]. In these works [6–9,17–19,21], flat transmitters were fabricated and tested.

To generate HIFU, especially for high-frequency one, laser-generated focused ultrasound (LGFU) is an alternative approach by fabricating concave LGUS transmitters on the concave surface of a lens, usually called a photoacoustic lens, for acoustic focusing [5,10–12,16,20,23,26,27]. It has been demonstrated that the photoacoustic lens is able to produce a tight HIFU focal volume of 75 μm and 400 μm in lateral and axial directions, respectively, and can be applied to high-precision targeted therapy [5]. However, in all these demonstrations [5,10–12,16,20,23,26,27], light illumination should be well aligned with the photoacoustic lens on optical tables, which is not applicable to handheld operation. Hence, employing the LGFU for intraoperative therapy in clinical use is also highly restricted. Furthermore, most of the LGFU photoacoustic lens employed carbon nanotubes (CNTs)-PDMS transmitters [5,10–12,16,20,23,26], where the as-grown CNTs require expensive manufacturing equipment and complicated fabrication process. Although fiber-optic LGUS devices were investigated, only diverging ultrasound or an acoustic pencil beam was demonstrated [14,15,22,24,28]. That is, a miniature fiber-optic device capable of HIFU generation has not been demonstrated. Because such a HIFU device can perform high-precision therapy for intraoperative applications, it is of great clinical value.

In this letter, for the first time to our knowledge, a miniature fiber-optic HIFU device based on photoacoustic transduction is presented. A simple low-cost method for fabricating the photoacoustic lens for efficient HIFU generation is developed. The diameter of the HIFU device is 6.5 mm and a tight focal volume of ~100 μm and ~500 μm in the lateral and axial directions, respectively, is achieved. The peak positive pressure is up to >30 MPa. Specifically, in contrast to existing works on HIFU generation using the CNTs-PDMS photoacoustic lens [5,10–12,16,20,23,26], the novelty of this work lies in two parts: (i) a miniature fiber-optic HIFU device facilitating intraoperative applications and handheld operation; (ii) a simple low-cost fabrication method of the photoacoustic lens that can also achieve great performances regarding the HIFU pressure level within a tiny focal spot size.

2. Methods

2.1 Fabrication and characterization of photoacoustic lens

We used a candle with diameter of 15 mm to produce CSNPs at room temperature by a process of flame synthesis [18]. The process was begun after the candle flame became stable with a flame height of ~3 cm. To produce focused ultrasound, we used a plano-concave optical lens (45006, Edmund), serving as the photoacoustic lens in this work, with a diameter of 6 mm and a radius of curvature of 4.71 mm. As shown in Fig. 1(a), the lens was placed within the flame core at ~3 cm above the wick for 6 seconds, and a uniform CSNPs layer was then coated on the curved surface of the lens. To enable efficient photoacoustic conversion, PDMS was further coated to make CSNPs-PDMS composites. A PDMS base and a curing agent (Sylgard 184, Dow Corning) were mixed at a ratio of 10:1. Spin coating of PDMS was

Optics EXPRESS

used in fabricating CNTs-PDMS photoacoustic lens [5]. However, we found that the adhesion of the CSNPs layer to the substrate of the lens is poor, and the liquid PDMS will lift and float the CSNPs layer from the substrate by spin coating. That is, spin coating cannot be adopted in our case. Thus, a dip-coating process was developed. As shown in Fig. 1(b), the lens with the CSNPs layer was mounted on a post holder and immersed in a liquid PDMS pool. The optical axis of the lens was along the horizontal direction. The other side of the post was connected to a motorized stage (not shown in Fig. 1(b)) to lift the lens from the PDMS pool at a low speed of 5 μm/s along the vertical direction. During the dip-coating process, the liquid PDMS penetrated into the CSNPs layer by virtue of its porous structure [18]. After the dip-coating process, the thickness of the pure PDMS layer (i.e., without CSNPs) was >45 μm, which is much thicker than that of the CSNPs layer of ~12 μm (thickness measurement described later). The pure PDMS layer will cause severe attenuation of LGUS, especially for high-frequency components [13]. Thus, we tried to remove the surplus PDMS by four steps. (i) The lens with the CSNPs-PDMS composite was mounted on a post holder (as shown in Fig. 1(c)), which is connected to a rotation stage (not shown in Fig. 1(c)). The rotation stage can perform lens rotation with the center of the lens as the center of rotation. The optical axis of the lens was also along the horizontal direction. (ii) The lens was rotated by 90° and placed for 30 mins. The surplus PDMS will flow downward (indicated by the blue arrow in Fig. 1(c)) to the downside of the lens due to the gravitational force. (iii) Tissue paper was used to wipe out the surplus PDMS from the downside of the lens. (iv) Steps (ii) and (iii) were repeated for 4 times. The above method can significantly reduce the thickness of the pure PDMS layer to ~12 μm (described later). Finally, the PDMS was cured at 60 °C for 90 mins. Figure 1(d) shows the picture of the fabricated CSNPs-PDMS photoacoustic lens.

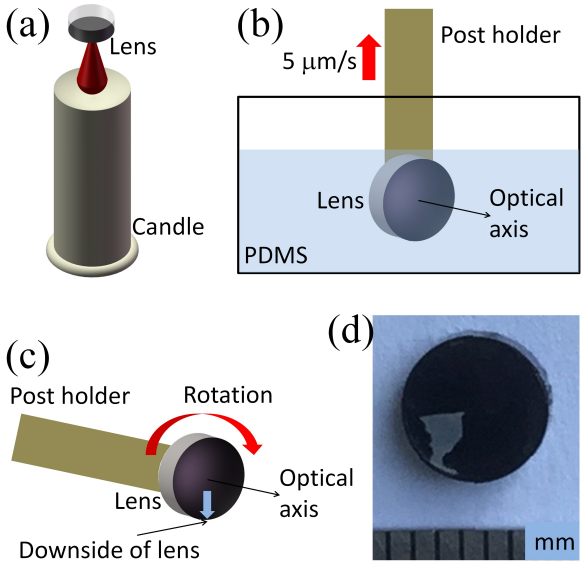

Fig. 1. (a) The lens placed above the candle in the process of flame synthesis. (b) Schematic of dip-coating process. (c) Schematic of removing the surplus PDMS. (d) Picture of the fabricated CSNPs-PDMS photoacoustic lens. The light region at the bottom left part of the lens is simply due to light reflection when taking the picture.

To characterize the thickness of the CSNPs-PDMS composite, scanning electron microscopy (SEM) can be used. It is challenging to observe the cross section of the CSNPs-PDMS composite on the lens using SEM due to the difficulty in cutting the lens. Thus, we used a laser scanning confocal microscope (LSM 700, ZEISS) instead. Since light cannot penetrate through the CSNPs layer, only the thickness of the area containing PDMS only can be measured. In this regard, we prepared two samples to deduce the respective thickness of

Optics EXPRESS

the CSNPs layer and the pure PDMS layer of the CNSPs-PDMS composite. The first sample was dip coated with PDMS only. The second sample was coated with CSNPs on half space of the lens and then dip coated with PDMS. The schematics of the two samples are shown in Figs. 2(a) and 2(b). Note that the fabrication conditions of CSNPs coating and PDMS coating were the same as mentioned above. As shown in Figs. 2(a) and 2(b), the PDMS thickness of the first sample is 11.2 μm and that of the second sample in the area with PDMS only is 22.6 μm. Thus, we can deduce that the thickness of the CSNPs layer is 11.4 μm, and that of the pure PDMS layer is 11.2 μm. To double check the thickness of the CSNPs layer and the pure PDMS layer by SEM, we made the CSNPs-PDMS composite on a flat glass substrate under the same fabrication conditions as mentioned above. The flat glass can be cut easily. After cutting the flat glass coated with the CSNPs-PDMS composite, its cross section can thus be studied by SEM, as shown in Fig. 2(c). As can be seen, the thickness of the CSNPs layer is 12.1 μm, and that of the pure PDMS layer is 12.4 μm, which are in good agreement with the values by using the confocal microscope for the case of the lens. This is reasonable considering the same fabrication conditions for the two cases of the CSNPs-PDMS composite on the lens and on the flat glass. Furthermore, the morphology and structure of the CSNPs were studied by SEM. As shown in Fig. 2(d), the particle size of the CSNPs is uniform with a diameter of ~40 nm.

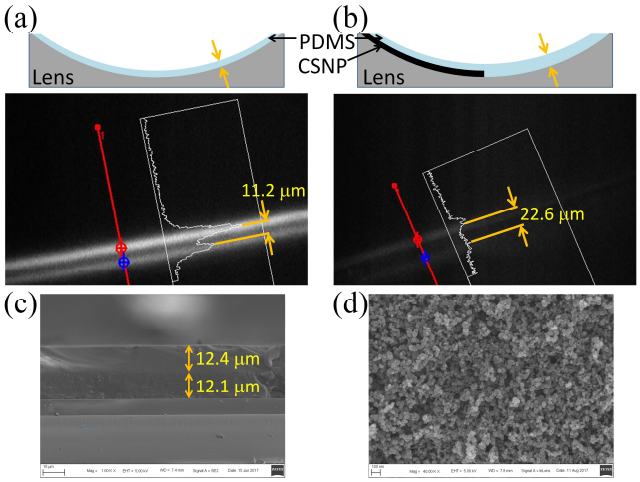

Fig. 2. (a) The first sample coated with PDMS only; the PDMS thickness measurement by the confocal microscope. (b) The second sample coated with CSNPs on half space of the lens and then coated with PDMS; the PDMS thickness measurement by the confocal microscope. (c) SEM picture of the cross section of the CSNPs-PDMS composite on the flat glass. (d) SEM picture of the morphology and structure of the CSNPs.

To check the thickness homogeneity of the coated CSNPs-PDMS composite, the thickness measurement by the confocal microscope (as demonstrated in Figs. 2(a) and 2(b)) was conducted for 4 different points chosen randomly. The measured thickness was 22.9 ± 1.7 (standard deviation), which shows satisfactory thickness homogeneity of the CSNPs-PDMS coating on the lens. Another indirect evidence of the thickness homogeneity is shown in Fig. 2(c), where nearly the same thickness of the CSNPs-PDMS coating (over a length of ~0.12 mm) on the flat glass was observed.

2.2 Fiber-optic HIFU device and system

As mentioned above, a miniature fiber-optic device facilitates handheld operation and enables intraoperative applications. Thus, a multi-mode fiber (FT1500UMT, Thorlabs) with a core diameter of 1500 μm was integrated with the CSNPs-PDMS photoacoustic lens. The design is illustrated in Fig. 3(a). Overall, a tube can be used to fix the fiber and the lens using epoxy. In

Optics EXPRESS

fabrication, because the sizes of the fiber and the lens differ much, one steel tube and two glass tubes were used to facilitate the integration and coaxial alignment. Figure 3(b) shows the picture of the fabricated HIFU device. A suitable distance (~30 mm) between the tip of the fiber and the lens was chosen to ensure that the beam emitted from the fiber can be expanded to the size similar to the lens aperture (i.e., the laser beam can fully cover the lens), which was tested experimentally. The outermost steel tube has inner diameter of 6.1 mm and outer diameter of 6.5 mm. Currently, the diameter of the HIFU device is mainly limited by the size of the lens.

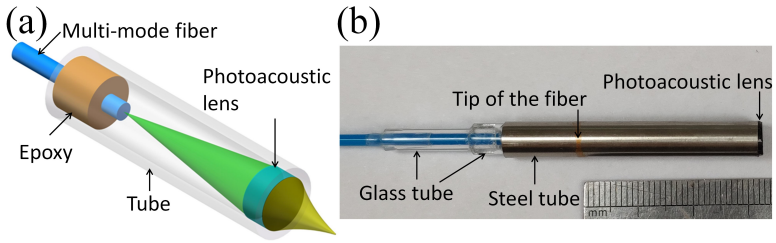

Fig. 3. (a) Schematic of the HIFU device. (b) Picture of the fabricated HIFU device. The position of the tip of the fiber is indicated. The distance between the fiber tip and the photoacoustic lens is ~30 mm.

The damage threshold of the fibers with either small or large cores is the same, which is ~5 GW/cm^2 for optical power densities (see Thorlabs website). Thus, large core fibers allow delivery of high optical power. Considering the same pulsed energy for laser illumination on the photoacoustic lens, large core fibers allow delivery of laser with high pulse repetition rate (i.e., high optical power) and thus high LGFU power for therapy, which is desired for therapy. Therefore, the large core fiber was used.

Figure 4 shows the experimental setup for characterization of the fiber-optic HIFU device. A 6-ns pulsed laser (532 nm, Q-smart 450, Quantel) with a repetition rate of 20 Hz was used. The laser was attenuated by neutral density filters and then coupled into the fiber using a focusing lens. The laser energy for photoacoustic excitation can be controlled by setting the attenuation of the neutral density filters. The ultrasound pressure was measured by a home-built fiber-optic hydrophone (FOH) [30], whose sensitivity was calibrated as ~4.9 mV/MPa at 10 MHz in advance using an acoustic source with known pressure levels (peak positive: 0.2 MPa; peak negative: 0.34 MPa) generated by a 10 MHz focused ultrasound transducer (focal length: 15 mm, V327-SU, Panametrics NDT, MA). The pressure levels of the 10 MHz focused ultrasound transducer was calibrated using a commercial hydrophone (HGL-0085, ONDA). A fiber circulator was used for convenient access to both the input and output of the FOH. The FOH was probed by a continuous-wave laser (HP 8168F, Agilent), and the reflected laser power was split into two parts with a power ratio of 10:90. The 10% reflected power was monitored by a power meter (2832-C, Newport), and the 90% power was measured by a photodetector (1811-FC-AC, New Focus). The signal from the photodetector was recorded by a digital oscilloscope (HDO4024, LeCroy). Both the HIFU device and the FOH were immersed in water for sound coupling. The FOH was mounted on a motorized three-dimensional stage for ultrasound field measurements. Our FOH has a small active sensing area (~8 μm in diameter), which makes the FOH suitable to measure ultrasound fields with high spatial resolution. For cavitation demonstration, the 10 MHz focused transducer (V327-SU) was used as a detector and placed with its axis orthogonal to the axial direction of the HIFU device.

Optics EXPRESS

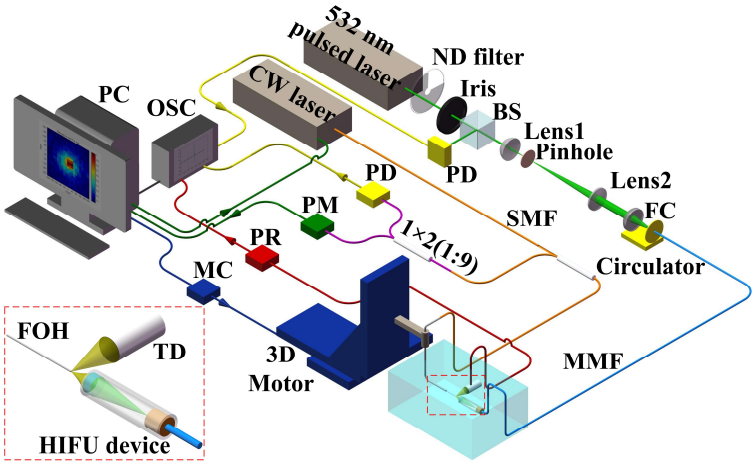

Fig. 4. Experimental setup for characterization of the HIFU device. Inset: illustration of the alignment of the HIFU device, the FOH, and the focused transducer for cavitation demonstration.; BS, beam splitter; FC, fiber coupler; MC, motor controller; MMF, multi-mode fiber; ND, neutral density; OSC, oscilloscope; PC, personal computer; PD, photodetector; PM, power meter; PR, pulser/receiver; SMF, single-mode fiber; TD, transducer.

3. Results

3.1 Calibration

We first measured the time-domain pressure waveforms generated by the fiber-optic HIFU device. We scanned the FOH to find out the acoustic focal point (more details described later). The focal length of 4.9 mm was then determined. Figure 5(a) shows the measured pressure waveforms when the FOH was at the focal point (z = 4.9 mm) and an out-of-focus point (z = 4.6 mm) along the axial direction. The normalized frequency spectra of the two waveforms are shown in Fig. 5(b). The bandwidth at −6 dB was ~14 MHz for the pressure waveform at the focal point. According to Ref [5], the effective focal gain of our CSNPs-PDMS photoacoustic lens was calculated as 62 at a 14-MHz frequency, which is similar to the focal gain of 54 of the CNTs-PDMS photoacoustic lens [5].

Second, we characterized the relationship between the acoustic pressure levels and the pulsed laser energy. The laser energy from 0 to ~8.4 mJ was used. The tip of the FOH was placed at the focus of the HIFU device to measure its maximum pressure. Both the peak positive and peak negative pressure values were recorded, as shown in Fig. 5(c). The peak positive pressure achieves HIFU pressure levels of ~33 MPa at pulsed energy of ~8.4 mJ, corresponding to laser fluence of 29.7 mJ/cm^2. Besides, the peak positive pressure values were saturated when the laser fluence exceeded ~30 mJ/cm^2. The saturation laser energy fluence is close to the reported value from the flat CSNPs-PDMS composite film [18]. The mechanism of the saturation is under investigation. On the other hand, the peak negative pressure up to 5.7 MPa was measured at pulsed energy of ~0.66 mJ. When the laser energy was further increased, acoustic cavitation occurred at the tip of the FOH, which will be described in detail later. The damage threshold of the CSNPs-PDMS composite film coated on the photoacoustic lens was measured to be ~23 mJ (i.e., ~81 mJ/cm^2).

Third, the focal volume of the fiber-optic HIFU device was measured. The FOH was scanned over the focal plane at step size of 20 μm. The peak-to-peak pressure field distribution in the focal plane is shown in Fig. 5(d), where the −6 dB focal size of ~100 μm in the lateral direction can be determined. To further check the focal spot size in the axial direction, the FOH was scanned along the axial direction. The measured peak positive and peak negative amplitudes are shown in Fig. 5(e). From the one-dimensional profile, the −6 dB focal size in the axial direction was estimated to be ~500 μm (diameter). The positive

Optics EXPRESS

pressure was larger than the negative pressure within the focal volume. A similar phenomenon of larger peak positive pressure was reported using a CNTs-PDMS photoacoustic lens [5]. The results shown in Figs. 5(a), 5(b), and 5(e) were obtained under laser fluence of ~2.3 mJ/cm^2 and Fig. 5(d) under laser fluence of ~0.8 mJ/cm^2.

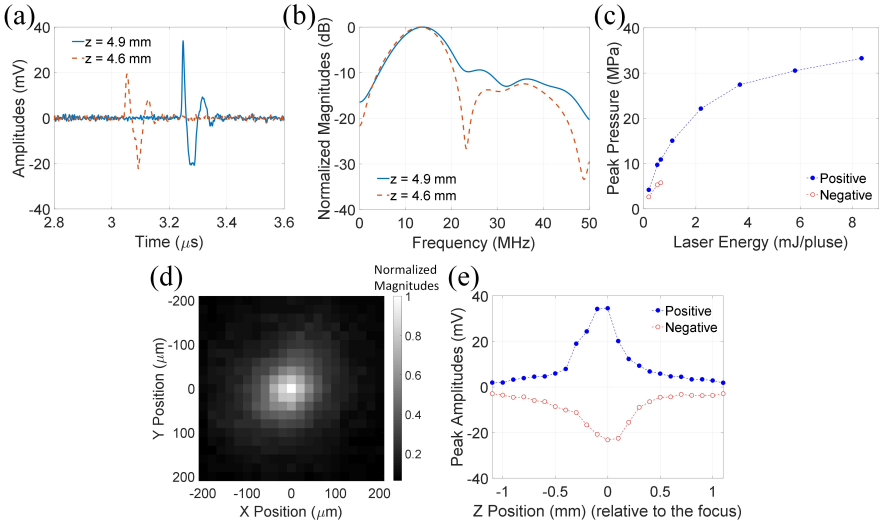

Fig. 5. (a) Measured pressure waveforms by FOH at the focal point (z = 4.9 mm) and the out-of-focus point (z = 4.6 mm). (b) Normalized frequency spectra of (a). (c) Peak positive and peak negative pressure values versus laser energy at the focal point (z = 4.9 mm). (d) Spatial profile in the focal plane (z = 4.9 mm). (e) Axial profile along the z direction. Z Position is relative to the focus (z = 4.9 mm).

3.2 Acoustic cavitation demonstration

Acoustic cavitation produced by the fiber-optic HIFU device was demonstrated. We basically repeated the cavitation experiment demonstrated in [16,23] by using our HIFU device. The details of the experiment in [16,23] and the interpretation of its experimental results can be found in [16,23]. Our experimental setup (similar to that in [23]) is shown in Fig. 4, and the arrangement of the HIFU device, the FOH, and the 10 MHz focused ultrasound transducer (V327-SU) is shown in the inset of Fig. 4. The FOH was placed at the focal point of the HIFU device.

The generated time-domain pressure waveforms measured by the FOH were recorded under different laser energy levels. Several representative waveforms are shown in Fig. 6(a). For the low energy level (0.66 mJ/pulse), comparable positive and negative amplitudes were observed, while for higher energy levels (2.2 and 5.8 mJ/pulse), much stronger negative amplitudes were measured, which indicates bubble formation at the surface of the tip of the FOH according to the reported results in [16] (i.e., a bubble at solid surfaces in water; see Fig. 6 in [16] and its related explanation). Besides, the temporal durations of the negative amplitudes are longer as increased laser energy levels. The phenomenon is consistent with the reported results in [16], which is another evidence of the bubble formation.

We also checked acoustic cavitation recorded by the 10 MHz focused ultrasound transducer, as shown in Fig. 6(b). The pulsed laser was used as the trigger for signal acquisition by the transducer. Figure 6(b) shows two representative time-domain pressure waveforms under the laser energy levels of 0.53 mJ/pulse (without bubbles) and 3.7 mJ/pulse (with bubbles), respectively. In Fig. 6(b), Sig1 is the HIFU pressure signal scattered by the FOH and then detected by the transducer. As can be seen, Sig1 appeared at ~15.3 μs, which is approximately the time for sound to travel from the photoacoustic lens to the FOH and then from the FOH to the transducer. Another delayed pressure signal, Sig2, is due to an additional

Optics EXPRESS

round-trip reflection between the FOH and the HIFU device. As can be seen, Sig1 appeared at ~15.3 μs, and Sig2 appeared at ~21.6 μs, which is delayed by ~6.3 μs with respect to Sig1, corresponding to a distance of ~9.5 mm considering the speed of sound in water as 1500 m/s. The distance is close to the round-trip distance between the FOH and the HIFU device (9.8 mm). It is reasonable that the amplitudes of Sig1 and Sig2 for the case of 0.53 mJ/pulse are smaller than those for 3.7 mJ/pulse. Interestingly, Sig3 and Sig4 were only presented at high laser energy level of 3.7 mJ/pulse. According to [23], they are cavitation-induced signals (see Fig. 4 in [23] and its related explanation), and Sig3 and Sig4 are the first and the second collapses of cavitation bubbles, respectively. Besides, T1 is the time from the initial bubble nucleation to its first collapse (Sig3), and T2 is the time from the first collapse to the second collapse (Sig4) [23]. T1 and T2 represent bubble lifetimes of cavitation occurrences [23].

A statistical study of T1 and T2 under several laser energy levels (2.2–11.4 mJ) was also conducted by acquiring 100 measurements at each laser energy level. As shown in Fig. 6(c), both T1 and T2 become longer as the increased laser energy levels, which is also consistent with the reported observations [23]. Note that at the laser energy level of 2.2 mJ, only the first bubble collapse was observed.

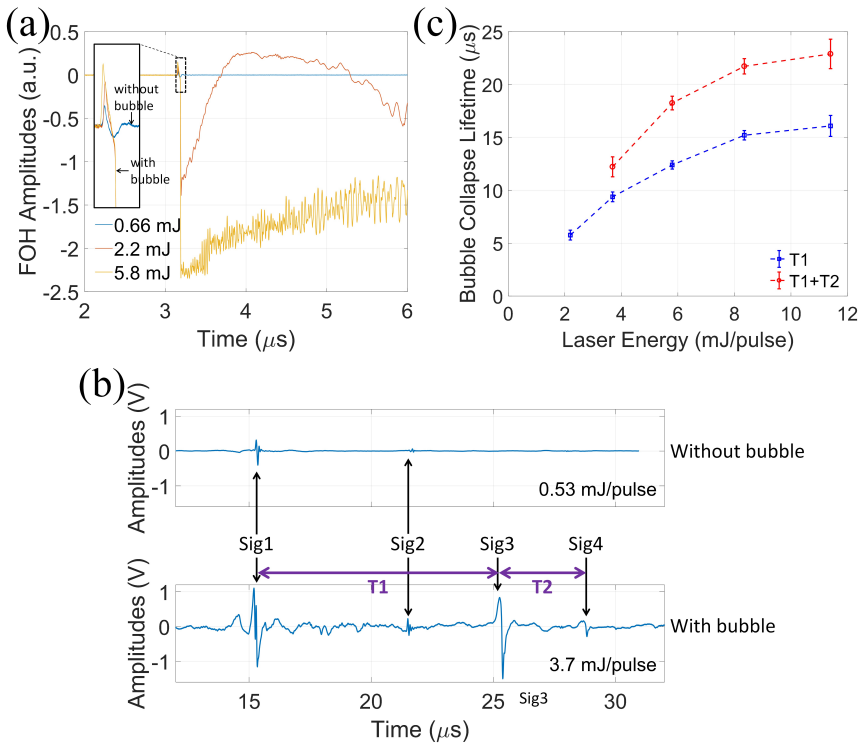

Fig. 6. (a) Representative time-domain pressure waveforms measured by FOH. (b) Representative time-domain pressure waveforms measured by the transducer at laser energy levels of 0.53 mJ/pulse (without bubbles) and 3.7 mJ/pulse (with bubbles). (c) Statistical study of bubble collapse lifetimes.

4. Discussion and conclusion

The HIFU conversion efficiency can be evaluated by the slope of peak pressure vs. laser energy (see Fig. 5(c)). Typically, there are two slopes for low-energy and high-energy laser excitation regimes for the LGFU photoacoustic lens [23]. The *f*-numbers of the lenses used in Ref [5]. (aperture diameter: 6 mm), our HIFU device, and Ref [23]. (aperture diameter: 15 mm) are 0.92, 0.79, and 0.61, respectively. The slopes (peak pressure vs. laser energy) of Ref

Optics EXPRESS

[5], our HIFU device, and Ref [23]. are ~2 MPa/mJ, >10 MPa/mJ, and ~20 MPa/mJ, respectively, for low-energy laser excitation regime, and are ~0.4 MPa/mJ, ~2 MPa/mJ, and 2 MPa/mJ, respectively, for high-energy one. The HIFU conversion efficiency increases as the *f*-number decreases, which is consistent with the reported findings in [23]. It is worth mentioning that higher HIFU pressure of the proposed HIFU device may be achieved by reducing the thickness of the excess pure PDMS layer (Fig. 2(c)), which simply attenuates the ultrasound pressure.

Piezoelectric transducers typically generate HIFU at low operating frequencies (a few MHz) due to the large aperture of the transducers [31]. LGFU transmitters are able to produce HIFU at tens of MHz [5,10–12,16,23,26,27]. For high-frequency HIFU (tens of MHz), several applications have been demonstrated. Targeted cell removal and cell membrane disruption were realized by the LGFU of ~30 MPa (several to tens of pulses used at 20 Hz) [5,12]. Micro-scale fragmentation of solid materials was demonstrated by the LGFU of ~30–40 MPa (1–1000 pulses used at 20 Hz) [5]. Cleaving of cell clusters by the LGFU of >50 MPa, and ablation of tissues (intestinal cell spheroids and pig eyeball) by the LGFU of ~70 MPa were reported [11,26]. Note that all the above quoted pressure values are peak positive pressure. Thus, the HIFU pressure levels of ~33 MPa achieved in this work can be applied to some of the above-mentioned applications although higher pressure levels are desired. Besides, as described, the LGFU operated at a repetition rate of 20 Hz has demonstrated several applications. For example, LGFU of 1–1000 pulses at 20 Hz was used in Refs [5,12]. That is, it took 50 ms to 50 sec, which is considered realistic in a clinical setting. Thus, the laser repetition rate of 20 Hz (used in this work) is sufficient and realistic for several applications, although the LGFU at a high repetition rate (i.e., high LGFU power) is always desired for therapy.

A tight HIFU focal volume is favorable for free-field cavitation. According to [10], the probability of free-field cavitation is only 0.06% by the LGFU of ~50 MPa with a similar HIFU focal volume to ours. On the other hand, according to [23], the probability of free-field cavitation is up to 50% by the LGFU of ~60 MPa with a roughly half HIFU focal volume compared with ours. Thus, to achieve free-field cavitation by our HIFU device, the pressure level and the HIFU focal volume should be further enhanced and reduced, respectively. Alternatively, a spatio-temporal superposition approach of two ultrasound pulses might be used to realize free-field cavitation by our HIFU device at low LGFU of ~30 MPa [10].

The current HIFU device has a diameter of 6.5 mm, which can be used for intraoperative applications. To facilitate intracavitary applications, further miniaturization is needed. According to the study in [23], the reduction of the HIFU pressure level at the focus is approximately proportional to that of the aperture size considering the same *f*-number of the photoacoustic lenses. Thus, we expect that a ~3 mm HIFU device may be achievable by improving the HIFU conversion efficiency by ~2 times using the following two approaches. First, as mentioned in the last paragraph, the HIFU pressure can be further boosted by reducing the thickness of the excess pure PDMS layer (Fig. 2(c)). Second, a low *f*-number photoacoustic lens can be used to enhance the HIFU pressure at the expense of the working distance (mainly determined by the radius of curvature of the photoacoustic lens). Technically, the miniaturization will be ultimately limited by the HIFU conversion efficiency and the finite working distance (i.e., *f*-number) needed for practical applications.

The high HIFU pressure level will be compromised in soft tissue, especially for high-frequency HIFU. Take muscle tissue for example. The frequency-dependent attenuation coefficients of muscle tissue and water are ~1 dB/(cm·MHz) and 2.2×10^{-3} dB/(cm·MHz^2), respectively [5,32]. Thus, considering the same propagation distance (4.9 mm) for 14-MHz HIFU, extra acoustic attention of ~7 dB will be introduced. What is worse, the focal spot size (and focal volume) of HIFU will be increased due to the extra attenuation, which is not desired for high-precision therapy. Besides further boosting the HIFU pressure through technical advancement, one possible solution is decreasing the operating frequency at the

Optics EXPRESS

expense of the tiny focal spot size. By changing the operating frequency, the trade-off between HIFU pressure and focal spot size (or volume) imposes limits on the applicability of the HIFU device for high-precision therapy and may be optimized depending on different therapeutic applications.

Piezoelectric HIFU transducers typically have a narrow bandwidth for efficient sound generation. By contrast, the photoacoustic HIFU device generates wideband signals (as demonstrated in Fig. 5(b)). The wideband signal enables a tight HIFU focal volume in the axial direction, which can be useful in particular applications such as free-field cavitation [23]. However, for applications where a tiny HIFU focal spot size along the lateral plane is the key factor (i.e., the axial size is minor), the high-frequency part in the wideband signal of the photoacoustic HIFU device will simply introduce more attenuation of sound intensity. The approach of multilayer LGUS transmitters may provide a solution to fabricate the photoacoustic HIFU device for generating narrowband signals [21].

The fabrication of the CSNPs-PDMS photoacoustic lens can be divided into 3 steps: flame synthesis, dip coating, and surplus PDMS removal. Technically, it is possible to conduct each step in batch. (e.g., multiple candles can be used in step 1; multiple lenses can be immersed in a large pool of liquid PDMS in step 2; multiple lenses can be rotated together by a rotation stage.) Thus, batch fabrication of the photoacoustic lens may be feasible.

LGUS is a promising method to implement hybrid ultrasound and photoacoustic imaging systems and probes [21,28,33–35]. Since the demonstrated HIFU device is based on LGUS transmitters, it has potential to be further developed to realize ultrasound and/or photoacoustic image-guided HIFU therapy by utilizing the pulsed laser for ultrasound generation and photoacoustic excitation for ultrasound and photoacoustic imaging, respectively. The development is of clinical significance. The preliminary potential design of photoacoustic image-guided HIFU probe is discussed. As shown in Fig. 7, the left part, mainly consisting of a microelectromechanical-systems (MEMS) mirror for light scanning and a fiber-optic Fabry-Perot (FP) ultrasound sensor for photoacoustic detection [28], is for photoacoustic imaging, and the right part is the HIFU device.

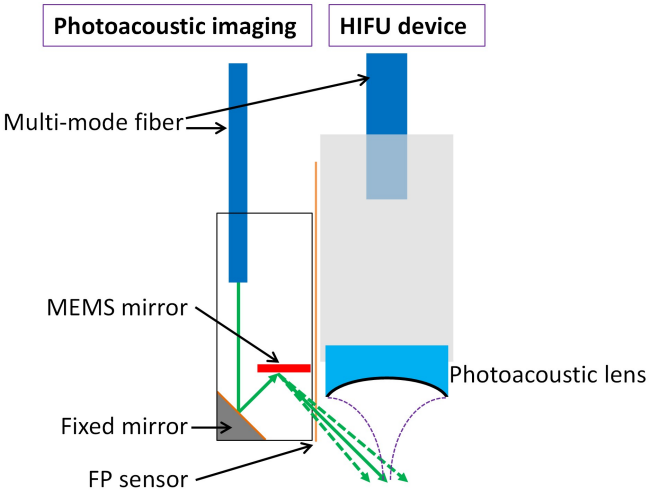

Fig. 7. Potential design of a photoacoustic image-guided HIFU probe.

In summary, we designed, fabricated, and characterized the first fiber-optic HIFU device using the CSNPs-PDMS composite-coated photoacoustic lens. Its fabrication is relatively simple and cost-effective. Acoustic cavitation was observed and studied. The HIFU pressure of ~33 MPa within a tiny focal spot size of ~100 μm allows high-precision therapy. Integration of the optical fiber facilitates handheld operation of the miniature HIFU device. Table 1 shows the comparison of existing LGUS transmitters, which elucidates the

Optics EXPRESS

advantages of this work. First, neither flat-film nor fiber-optic LGUS transmitters produce HIFU pressure within a tight focal volume. Thus, they are not suitable for therapeutic applications. Second, the photoacoustic lens by free-space laser illumination hampers the handheld operation and clinical applications. Third, the CNTs-PDMS-coated photoacoustic lens requires relatively expensive equipment and complicated fabrication process. In contrast, the demonstrated miniature HIFU device is capable of handheld operation, which is expected to open up versatile applications related to intraoperative high-precision therapy.

Table 1. Comparison of LGUS Transmitters

Technology		LGUS[a]				
	Miniature handheld device	Pressure (MPa) @ laser energy (mJ)	–6-dB bandwidth (MHz)	LGFU spot size (μm)	Transmitter material	Refs.
Flat film	–	~12 @ 4.2[b] [17]	7.6 [17]	–	Metallic or carbon-based absorbers	[6–9,17–19,21]
Fiber optic	YES	~0.8 @ ~0.01[c] [22]	29 [22]	–	Metallic or carbon-based absorbers	[14,15,22,24,28]
Photoacoustic lens	–	>50 @ >50 [5]	~15 [5]	75 [5]	CNTs-PDMS	[5,10–12,16,20,23,26]
Fiber optic & photoacoustic lens	YES	~33 @ ~8.4	~14	~100	CSNPs-PDMS	This work

[a]For the technology of "Flat film" and "Fiber optic", the Ref. with the maximum measured peak positive pressure is quoted. For the technology of "Photoacoustic lens", the Ref. with comprehensive characterization of LGFU is quoted. [b]The laser beam diameter was 12 mm. [c]The fiber core diameter was 200 μm.

Funding

National Natural Science Foundation of China (NSFC) (61775134).

Acknowledgments

The authors would like to acknowledge Dr. Tian Yang at SJTU for allowing us to use an ultrasound detector based on surface plasmon resonance for testing the photoacoustic lens; however, the detector was not used in obtaining the presented results in this work.

References

1. R. O. Illing, J. E. Kennedy, F. Wu, G. R. ter Haar, A. S. Protheroe, P. J. Friend, F. V. Gleeson, D. W. Cranston, R. R. Phillips, and M. R. Middleton, "The safety and feasibility of extracorporeal high-intensity focused ultrasound (HIFU) for the treatment of liver and kidney tumours in a Western population," Br. J. Cancer **93**(8), 890–895 (2005).
2. S. Dromi, V. Frenkel, A. Luk, B. Traughber, M. Angstadt, M. Bur, J. Poff, J. Xie, S. K. Libutti, K. C. P. Li, and B. J. Wood, "Pulsed-high intensity focused ultrasound and low temperature-sensitive liposomes for enhanced targeted drug delivery and antitumor effect," Clin. Cancer Res. **13**(9), 2722–2727 (2007).
3. S. Y. Yeo, A. J. Arias Moreno, B. van Rietbergen, N. D. Ter Hoeve, P. J. van Diest, and H. Grüll, "Effects of magnetic resonance-guided high-intensity focused ultrasound ablation on bone mechanical properties and modeling," J. Ther. Ultrasound **3**(1), 13 (2015).
4. D. L. Miller and J. Song, "Tumor growth reduction and DNA transfer by cavitation-enhanced high-intensity focused ultrasound in vivo," Ultrasound Med. Biol. **29**(6), 887–893 (2003).
5. H. W. Baac, J. G. Ok, A. Maxwell, K.-T. Lee, Y.-C. Chen, A. J. Hart, Z. Xu, E. Yoon, and L. J. Guo, "Carbon-nanotube optoacoustic lens for focused ultrasound generation and high-precision targeted therapy," Sci. Rep. **2**(1), 989 (2012).
6. T. Buma, M. Spisar, and M. O'Donnell, "High-frequency ultrasound array element using thermoelastic expansion in an elastomeric film," Appl. Phys. Lett. **79**(4), 548–550 (2001).
7. Y. Hou, J. S. Kim, S. Ashkenazi, M. O'Donnell, and L. J. Guo, "Optical generation of high frequency ultrasound using two-dimensional gold nanostructure," Appl. Phys. Lett. **89**(9), 093901 (2006).
8. H. W. Baac, J. G. Ok, H. J. Park, T. Ling, S.-L. Chen, A. J. Hart, and L. J. Guo, "Carbon nanotube composite optoacoustic transmitters for strong and high frequency ultrasound generation," Appl. Phys. Lett. **97**(23), 234104 (2010).
9. S. H. Lee, M. Park, J. J. Yoh, H. Song, E. Y. Jang, Y. H. Kim, S. Kang, and Y. S. Yoon, "Reduced graphene oxide coated thin aluminum film as an optoacoustic transmitter for high pressure and high frequency ultrasound generation," Appl. Phys. Lett. **101**(24), 241909 (2012).

Optics EXPRESS

10. H. W. Baac, T. Lee, J. G. Ok, T. Hall, and L. Jay Guo, "Dual-frequency focused ultrasound using optoacoustic and piezoelectric transmitters for single-pulsed free-field cavitation in water," Appl. Phys. Lett. **103**(23), 234103 (2013).
11. H. W. Baac, T. Lee, and L. J. Guo, "Micro-ultrasonic cleaving of cell clusters by laser-generated focused ultrasound and its mechanisms," Biomed. Opt. Express **4**(8), 1442–1450 (2013).
12. H. W. Baac, J. Frampton, J. G. Ok, S. Takayama, and L. J. Guo, "Localized micro-scale disruption of cells using laser-generated focused ultrasound," J. Biophotonics **6**(11-12), 905–910 (2013).
13. S.-L. Chen, Y.-C. Chang, C. Zhang, J. G. Ok, T. Ling, M. T. Mihnev, T. B. Norris, and L. J. Guo, "Efficient real-time detection of terahertz pulse radiation based on photoacoustic conversion by carbon nanotube nanocomposite," Nat. Photonics **8**(7), 537–542 (2014).
14. X. Zou, N. Wu, Y. Tian, and X. Wang, "Broadband miniature fiber optic ultrasound generator," Opt. Express **22**(15), 18119–18127 (2014).
15. L. Belsito, E. Vannacci, F. Mancarella, M. Ferri, G. P. Veronese, E. Biagi, and A. Roncaglia, "Fabrication of fiber-optic broadband ultrasound emitters by micro-optomechanical technology," J. Micromech. Microeng. **24**(8), 085003 (2014).
16. T. Lee, H. W. Baac, J. G. Ok, H. S. Youn, and L. J. Guo, "Controlled generation of single microbubble at solid surfaces by a nanosecond pressure pulse," Phys. Rev. Appl. **2**(2), 024007 (2014).
17. B.-Y. Hsieh, J. Kim, J. Zhu, S. Li, X. Zhang, and X. Jiang, "A laser ultrasound transducer using carbon nanofibers–polydimethylsiloxane composite thin film," Appl. Phys. Lett. **106**(2), 021902 (2015).
18. W.-Y. Chang, W. Huang, J. Kim, S. Li, and X. Jiang, "Candle soot nanoparticles-polydimethylsiloxane composites for laser ultrasound transducers," Appl. Phys. Lett. **107**(16), 161903 (2015).
19. H. W. Baac, J. G. Ok, T. Lee, and L. J. Guo, "Nano-structural characteristics of carbon nanotube-polymer composite films for high-amplitude optoacoustic generation," Nanoscale **7**(34), 14460–14468 (2015).
20. T. Lee, H. W. Baac, J. G. Ok, H. S. Youn, and L. J. Guo, "Nozzle-free liquid microjetting via homogeneous bubble nucleation," Phys. Rev. Appl. **3**(4), 044007 (2015).
21. S.-Y. Hung, W.-S. Wu, B.-Y. Hsieh, and P.-C. Li, "Concurrent photoacoustic-ultrasound imaging using single-laser pulses," J. Biomed. Opt. **20**(8), 086004 (2015).
22. S. Noimark, R. J. Colchester, B. J. Blackburn, E. Z. Zhang, E. J. Alles, S. Ourselin, P. C. Beard, I. Papakonstantinou, I. P. Parkin, and A. E. Desjardins, "Carbon-nanotube–PDMS composite coatings on optical fibers for all-optical ultrasound imaging," Adv. Funct. Mater. **26**(46), 8390–8396 (2016).
23. T. Lee, J. G. Ok, L. J. Guo, and H. W. Baac, "Low f-number photoacoustic lens for tight ultrasonic focusing and free-field micro-cavitation in water," Appl. Phys. Lett. **108**(10), 104102 (2016).
24. E. J. Alles, S. Noimark, E. Zhang, P. C. Beard, and A. E. Desjardins, "Pencil beam all-optical ultrasound imaging," Biomed. Opt. Express **7**(9), 3696–3704 (2016).
25. S.-L. Chen, "Review of laser-generated ultrasound transmitters and their applications to all-optical ultrasound transducers and imaging," Appl. Sci. **7**(1), 25 (2016).
26. T. Lee, W. Luo, Q. Li, H. Demirci, and L. J. Guo, "Laser-induced focused ultrasound for cavitation treatment: toward high-precision invisible sonic scalpel," Small **13**(38), 1701555 (2017).
27. T. Lee and L. J. Guo, "Highly efficient photoacoustic conversion by facilitated heat transfer in ultrathin metal film sandwiched by polymer layers," Adv. Optical Mater. **5**(2), 1600421 (2017).
28. G. Li, Z. Guo, and S.-L. Chen, "Miniature all-optical probe for large synthetic aperture photoacoustic-ultrasound imaging," Opt. Express **25**(21), 25023–25035 (2017).
29. S. Noimark, R. J. Colchester, R. K. Poduval, E. Maneas, E. J. Alles, T. Zhao, E. Z. Zhang, M. Ashworth, E. Tsolaki, A. H. Chester, N. Latif, S. Bertazzo, A. L. David, S. Ourselin, P. C. Beard, I. P. Parkin, I. Papakonstantinou, and A. E. Desjardins, "Polydimethylsiloxane composites for optical ultrasound generation and multimodality imaging," Adv. Funct. Mater. **28**(9), 1704919 (2018).
30. J. E. Parsons, C. A. Cain, and J. B. Fowlkes, "Cost-effective assembly of a basic fiber-optic hydrophone for measurement of high-amplitude therapeutic ultrasound fields," J. Acoust. Soc. Am. **119**(3), 1432–1440 (2006).
31. Y.-F. Zhou, "High intensity focused ultrasound in clinical tumor ablation," World J. Clin. Oncol. **2**(1), 8–27 (2011).
32. V. R. Amin, "Ultrasonic attenuation estimation for tissue characterization," Master Thesis (1989).
33. J. Jose, R. G. H. Willemink, W. Steenbergen, C. H. Slump, T. G. van Leeuwen, and S. Manohar, "Speed-of-sound compensated photoacoustic tomography for accurate imaging," Med. Phys. **39**(12), 7262–7271 (2012).
34. J. Xia, C. Huang, K. Maslov, M. A. Anastasio, and L. V. Wang, "Enhancement of photoacoustic tomography by ultrasonic computed tomography based on optical excitation of elements of a full-ring transducer array," Opt. Lett. **38**(16), 3140–3143 (2013).
35. T. F. Fehm, X. L. Deán-Ben, and D. Razansky, "Four dimensional hybrid ultrasound and optoacoustic imaging via passive element optical excitation in a hand-held probe," Appl. Phys. Lett. **105**(17), 173505 (2014).